Quaternary Science Reviews 276 (2022) 107317

Contents lists available at ScienceDirect

Quaternary Science Reviews

journal homepage: www.elsevier.com/locate/quascirev

Southern Hemisphere controls on ITCZ variability in southwest Madagascar over the past 117,000 years

Stephen J. Burns [a, *], David McGee [b], Nick Scroxton [a, c], Christopher W. Kinsley [b], Laurie R. Godfrey [d], Peterson Faina [e], Lovasoa Ranivoharimanana [e]

[a] Department of Geosciences, 611 North Pleasant Street, University of Massachusetts Amherst, MA, 01003, USA
[b] Department of Earth, Atmospheric and Planetary Sciences, Massachusetts Institute of Technology, 77 Massachusetts Avenue, Cambridge, MA, 02139, USA
[c] School of Earth Sciences, University College Dublin, Belfield, Dublin 4, Ireland
[d] Department of Anthropology, 240 Hicks Way, University of Massachusetts Amherst, MA, 01003, USA
[e] Bassins sédimentaires, Evolution, Conservation, Université d'Antananarivo, Madagascar, BP 906, Antananarivo 101, Madagascar

ARTICLE INFO

Article history:
Received 21 September 2021
Received in revised form
3 December 2021
Accepted 4 December 2021
Available online 13 December 2021

Handling Editor: Mira Matthews

Keywords:
Speleothems
Paleoclimatology
Madagascar
Southern hemisphere
Millennial-scale climate variability
Last glacial period

ABSTRACT

Migration of the inter-tropical convergence zone, driven by changes in seasonal insolation and high northern latitude temperatures, is the primary control on tropical rainfall on geologic timescales. We test this paradigm using the timing of growth of stalagmites from southwest Madagascar to infer the timing of expansion of the ITCZ to the south at its southern limit. Over the past 117 ky, speleothems grew in the study area primarily when two conditions are met: summer insolation greater than the mean and relatively high Southern Hemisphere temperatures as indicted by maxima in Antarctic ice core oxygen isotope ratios. We observe little influence of Northern Hemisphere, millennial scale temperature variability on the pluvial periods. Further, we observe periods during which the ITCZ simultaneously expands or contracts in both hemispheres. Because Antarctic isotope maxima are periods of increased atmospheric CO_2, our results have implications for how tropical rainfall in the Southern Hemisphere might respond to global warming.

1. Introduction

Several decades of research on the paleoclimatology of the tropics have led to the 'antiphase' paradigm of tropical hydrological change in which the Northern and Southern Hemisphere tropics are alternately wetter or drier perfectly out of phase with one another (Cheng et al., 2012; Wang et al., 2014). Such antiphase behavior is observed at orbital (Cruz et al., 2005; Cheng et al., 2016) and millennial timescales (Wang et al., 2001, 2004; Kanner et al., 2012) in many regions of the tropics. At both timescales, antiphase behavior is attributed to meridional migration of the mean location of the intertropical convergence zone (ITCZ). At orbital timescales, ITCZ migration is driven by changes in the precession of Earth's orbit, with maximum summer insolation in the Northern Hemisphere necessarily coinciding with minimum summer insolation in the Southern Hemisphere. Changes in insolation also change the latent and sensible heat components of the monsoons, with Northern and Southern Hemisphere summer monsoons varying in phase with summer insolation in their respective hemispheres (Cheng et al., 2012; Wang et al., 2014).

Similarly, large amplitude changes in tropical hydrology at millennial timescales are observed during glacial periods, when rapid, high amplitude changes in temperature, ice sheet size and topography, sea ice extent and thermohaline circulation are observed. The impact of these changes in the tropics is observed to mirror changes in high northern latitude temperatures, particularly Dansgaard/Oeschger (D/O) cycles (Kanner et al., 2012; Wang et al., 2001), including on Socotra Island, in the Northern Hemisphere side of the Indian Ocean at almost the same longitude as the study area (Burns et al., 2003). Cold stadial periods in the Arctic are interpreted to result in a more southerly ITCZ position (Schneider et al., 2014), weakened Northern Hemisphere monsoons and

* Corresponding author.
E-mail addresses: sburns@umass.edu (S.J. Burns), davidmcg@mit.edu (D. McGee), nick.scroxton@ucd.ie (N. Scroxton), ckinsley@mit.edu (C.W. Kinsley), lgodfrey@umass.edu (L.R. Godfrey), petersonfaina@gmail.com (P. Faina), ranivolova@gmail.com (L. Ranivoharimanana).

https://doi.org/10.1016/j.quascirev.2021.107317
0277-3791/

strengthened Southern Hemisphere monsoons. These associations are particularly strong for stadial periods associated with Heinrich events (Wang et al., 2004). An influence of high southern latitude temperature change has also been observed in some Northern Hemisphere monsoon records of the last glacial. At the millennial scale the Asian Monsoon varies in an antiphase manner with Antarctic temperatures, with a strengthened monsoon associated with colder Antarctic temperatures (Cai et al., 2006; Rohling et al., 2009; Chen et al., 2016). Thus far, how the millennial-scale temperature variability recorded in Antarctic ice cores impacts the Southern Hemisphere tropics, if at all, is not clear.

While the antiphase paradigm accords with the great majority of tropical paleoclimate records, in eastern Africa some paleoclimate studies indicate simultaneous increases and decreases in rainfall on both sides of the equator from the Last Glacial Maximum (LGM) into the Holocene(Otto-Bliesner et al., 2014; Garelick et al., 2021). For example, during the LGM, conditions across eastern Africa were dry, including at Lake Malawi (9°–15° S) (Castañeda et al., 2009), Lake Victoria (1°N- 13° S) (Johnson et al., 1996) and Lake Rotundu (Garelick et al., 2021). Similarly, Stager et al. (2011) documented widespread drought conditions across equatorial eastern Africa during Heinrich event 1, including most sites south of the equator. Eastern African paleoclimate records from both sides of the equator are more similar than different for the early, mid- and late-Holocene time slices (Tierney et al., 2011), and a late Holocene climate record from northwest Madagascar is in phase at centennial timescales with northern Indian Ocean records (Scroxton et al., 2017). Several authors have proposed that SSTs in the western Indian Ocean are the dominant influence on rainfall patterns in eastern Africa from orbital to centennial timescales (Scroxton et al., 2017, 2019; Tierney et al., 2016). In contradiction to these studies, however, other paleoclimate records from southeastern Africa show antiphase behavior, with wet periods corresponding to cold periods in the Northern Hemisphere (Schefuβ et al., 2011; Tierney et al., 2008). And wet episodes recorded in Lake Malawi sediments occur near D/O events (Brown et al., 2007). A recently published marine record from the Mozambique Channel also indicated wet conditions for northwest Madagascar during Heinrich Event 1 and the Younger Dryas (Ma et al., 2021). Thus, there remains considerable uncertainty regarding the relationship between climate in eastern Africa and the southwest Indian Ocean region on one hand and Northern Hemisphere climate on the other. In addition, very few studies of climate in the region extend beyond the LGM, particularly with the dating certainty to investigate linkages between the Southern and Northern Hemispheres at millennial and orbital timescales (Brown et al., 2007).

To attempt to address these questions, we carried out a study of changes in tropical moisture availability at the southern limit of the tropics in southwest Madagascar from the recent to 117 ky BP. The study area is relatively arid, with rainfall near the minimum needed for speleothems to grow. Thus, we use the ages of speleothems that were growing relatively quickly to infer periods of increased rainfall relative to periods without speleothem growth.

1.1. Modern climate of Madagascar

Madagascar, the largest island in the Indian Ocean, lies mostly in the Southern Hemisphere tropics, from 12°S to 26°S latitude. The island's physiography is dominated by a mountain range that runs almost the length of the island along on its eastern side (Fig. 1). The mountains create a boundary to moisture carried by the low level southeast trade winds and lead to marked differences in the amount and seasonality of rainfall east to west across the island (Jury, 2003; Jury et al., 1995). The southeast trade winds control rainfall to the east of Madagascar's mountains, while to the west, the highlands produce a rain shadow and rainfall is highly seasonal with a strong North-to-South gradient in total annual rainfall (Fig. 2). Monthly rainfall is strongly influenced by seasonal changes

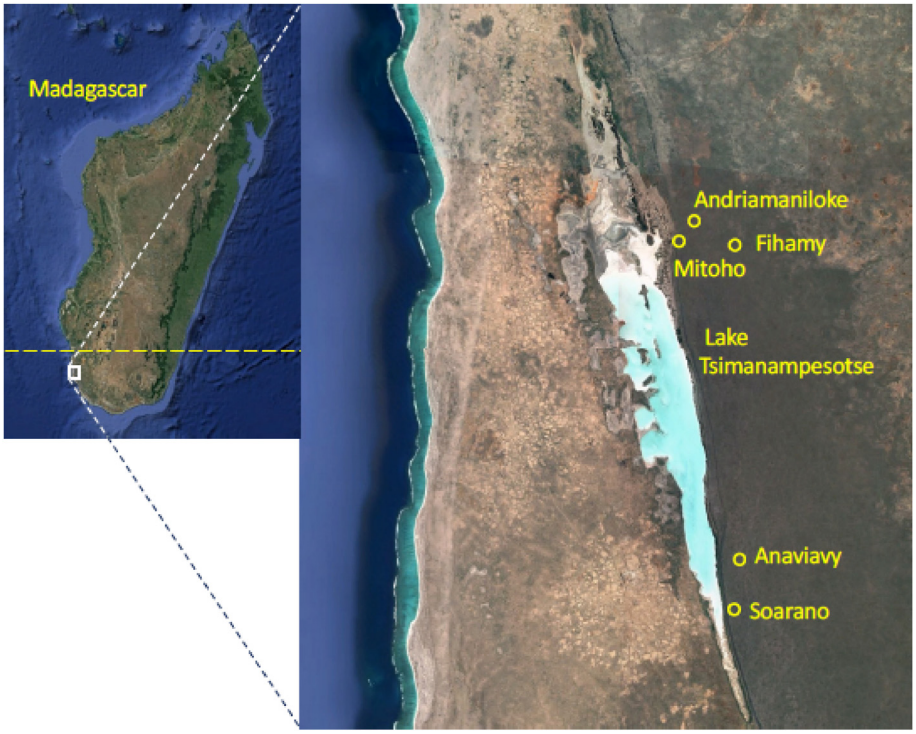

Fig. 1. Location of the study area and cave sampling sites. Dashed yellow line on inset map is the Tropic of Capricorn.

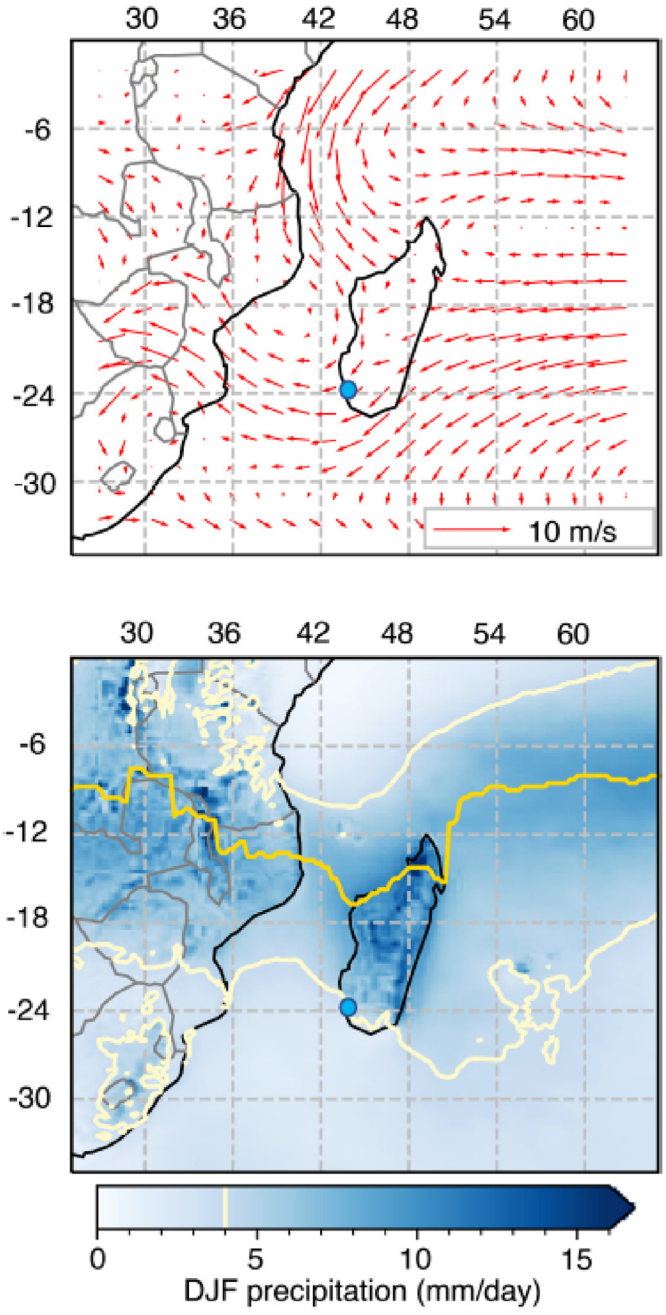

Fig. 2. Wind and precipitation for the studied region. Top figure is ERA5 850 hPa January mean wind direction and strength (red arrows) (Hersbach et al., 2020b). Bottom figure is ERA5 DJF mean rainfall (blue gradient) (Hersbach et al., 2020a) with 4 mm isohyet (light yellow line) to denote approximate extent of the tropical rainbelt and January mean ERA5 Outgoing Longwave Radiation minima (yellow line) to denote approximate position of the summer ITCZ. Blue circles mark study area.

in insolation and the migration of the ITCZ in the Indian Ocean (Jury, 2003). The western parts of the island experience a classical monsoonal climate with the northeast monsoon winds over the western tropical Indian Ocean re-curving over the northern Mozambique Channel to become rain-bearing northwesterlies in the austral summer months (Fig. 2) (Jury, 2015). As oceanic moisture is carried over the land, convection is induced by sensible heating of the land surface, which reinforces monsoonal flow (Jury, 2015). Rainfall is highly seasonal with generally 70% of total annual rainfall coming in December through February. During the height of the austral summer the ITCZ lies over central Madagascar reaching as far south as 17–20°S in February (Jury et al., 1995). Monthly rainfall amount is as high as 450 mm during summer in northwestern Madagascar (Jury et al., 1995), whereas in the much drier southwest, it ranges from about 50 to 200 mm per month at this time of year. Mean annual rainfall at Toliara, the nearest meteorological station to the study, area is around 400 mm, with 67% falling in DJF (Fig. 3). Mean annual temperature is 24 °C, averaging about 27 °C in January and 21 °C in July. The ecosystem in the study area is categorized as 'spiny bush', dominated by members of two plant families, the cactus-like Didiereaceae and the succulent Euphorbiaceae. Also characteristic of this region are baobab (family Malvaceae) and *Pachypodium* (family Apocynaceae) trees (Goodman et al., 2018). These plants are well-adapted to survive under hot and dry (subarid) and highly seasonal climate conditions.

1.2. Paleoclimate of Madagascar

Lake sediment cores from across Madagascar have been used to investigate past climate, including Lake Mitsinjo (Matsumoto and Burney, 1994) in the northwest, Lake Tritrivakely (Gasse and Van Campo, 1998; Gasse and van Campo, 2001) and Lakes Ampozolana and Kavitaha (Burney, 1987) in the Central Highlands, and Andolonomby (Burney, 1993) and Lake Ihotry (Vallet-Coulomb et al., 2006) in the southwest. These studies cover only the period from the mid- or late Holocene to recent, however, and are of fairly low resolution. On longer timescales remarkably little is known about the climate history of Madagascar. Lake Tritrivakely, which is located in the Central Highlands, has a sedimentary record that covers perhaps the past 150 ky, with a C-14 chronology covering the past 40,000 years (Gasse et al., 1994; Gasse and van Campo, 2001; Gasse and Van Campo, 1998). On a broad scale, the Tritrivakely record shows cooler conditions during glacial times, a deglacial warming in two steps, commencing at 17,000 and 15,000 cal yr B.P., and episodes of positive P–E balance from 38,000 to 32,000 and 17,000–9800 cal yr B.P. The LGM climate was interpreted to be drier than today.

Over the past few years several new speleothem-based paleoclimate studies of Madagascar have been published. Most of these have been from northwest Madagascar with a focus on the Holocene (Burns et al., 2016; Scroxton et al., 2017; Voarintsoa et al., 2017a, 2017b; Wang et al., 2019; Duan et al., 2021). Scroxton et al., (2019) reported on a deglacial record from the study area in southwest Madagascar. The results of the studies from northwest Madagascar differ with respect to relationships found between rainfall variability in that area versus the Northern Hemisphere western Indian Ocean region. Scroxton et al. (2017) showed in-phase changes in tropical hydrology in the two hemispheres over the past 1700 years. In contrast, Voarintsoa et al. (2017a, 2017b, 2019) and Duan et al. (2021) found evidence for antiphase relationship between the Northern and Southern Hemisphere monsoons (Voarintsoa et al., 2017a, 2017b, 2019; Duan et al., 2021). In particular, they found evidence fort a wetter climate in the region during the 8.2 ka event. Voarintsoa et al. (2017a, 2017b) concluded that rainfall in northwest Madagascar was linked to ITCZ migration, whereas Wang et al. (2019) suggested that ITCZ migration was not the sole or even primary determinant of climate in the area. Working in southwest Madagascar, Scroxton et al. (2019) found a

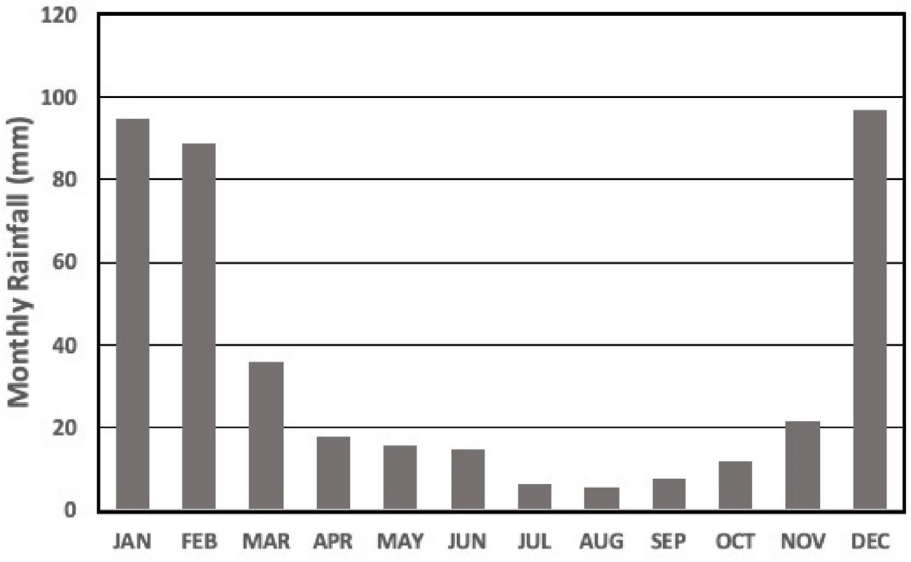

Fig. 3. Seasonal rainfall pattern at Toliara, 75 km N of study area, for the period 1980–2015.

strong connection to ITCZ movement on climate there but concluded that sea surface temperatures in the tropical western Indian Ocean were also important.

2. Material and methods

2.1. Study area

The study area, within Tsimanampesotse National Park, is at 24.10°S, 43.77°E, about 50 masl on a low, linear limestone escarpment 10 km from the west coast of Madagascar (Fig. 1). Caves are scattered throughout the escarpment, though large caverns are presently restricted to below the water table. We collected 18 individual stalagmites from five caves within this region. The majority of samples, 9, are from a single cave, Andriamaniloke. Three stalagmites, MT-2, MT-3 and MT-4 were recovered by divers from the flooded portion of Mitoho Cave. All others are from subaerial parts of caves. Stalagmites range in size from 12 cm to 65 cm (Appendix 1). Each stalagmite was cut along the growth axis and the cut surfaces were polished to better expose internal layering. Samples were inspected for any visible alteration or dissolution. No alteration was observable. All samples are composed entirely of calcite. Typical of this mineralogy, many samples are composed of visible, large columnar crystals from 1 to several 10s of cm in length, with the crystal long axis perpendicular to speleothem growth layers. Mineralogy was confirmed by X-ray diffraction analyses of powdered subsamples taken at the same locations as the subsamples used for age determinations. XRD analyses were conducted on a PANalytical X'Pert PW1821 X-ray diffractometer at the University of Massachusetts, Amherst.

2.2. Radiometric age determinations

For age determinations by the ^{230}Th/U method, subsamples of approximately 150 mg were initially drilled from the samples. Due to relatively low U contents, subsampling was later changed to removing chips of solid calcite of the same approximate weight; these chips were ultrasonicated in high-purity water three times to remove any contaminating powder from drilling before being dissolved. Between 1 and 14 age determinations were made per sample, the number depending primarily on stalagmite size (Table 1 and Appendix 1). The ^{230}Th/U isotopic analyses were made at the Massachusetts Institute of Technology. Samples weighing 79–432 mg were combined with a ^{229}Th–^{233}U–^{236}U tracer, digested, and purified via iron co-precipitation and ion exchange chromatography. Separate U and Th aliquots were analyzed using a Nu Plasma II-ES multi-collector ICP-MS equipped with a CETAC Aridus II desolvating nebulizer. Ages were corrected for initial ^{230}Th using an initial ^{230}Th/^{232}Th atomic ratio of $4.4 \pm 2.2 \times 10^{-6}$. Ages are presented on the ^{14}C timescale where 1950 CE or Common Era = 0 yr BP.

3. Results

The great majority of studies that use speleothems as paleoclimate archives rely on time series of oxygen isotope ratios or other geochemical proxies (Fairchild et al., 2006; Lachniet, 2009). Periods of speleothem growth have also been used as a paleoclimate indicator, specifically to infer sufficient available moisture for an active karst system (Fankhauser et al., 2016; Vaks et al., 2007). We apply the latter approach here. The results of 82 ^{230}Th/U age determinations on 18 different stalagmites reveal 26 discrete periods of speleothem growth lasting from a few hundred years to about 4000 years (Table 1 and Appendix 1). Five age determinations, one from AD-3, one from AD-11 and three from MT-3 were considered to be significant outliers and were not used to determine depositional ages. The ages of these samples were more than four standard deviations away from age depth curves determined by other samples from these speleothems. Also, for sample MT-3.

which was recovered from below the water table, the δ^{234}U values deviated significantly from other values for that stalagmites (Table 1). In six cases, a stalagmite grew in more than one interval of several thousand years separated by a much longer hiatus. The total range in ages of stalagmite growth extends from a recent, actively growing sample to a sample that grew at 116.9 ky BP (Fig. 4 and Table 1). The larger number of speleothems found in more recent time periods likely reflects a preservation bias for younger samples (Scroxton et al., 2016).

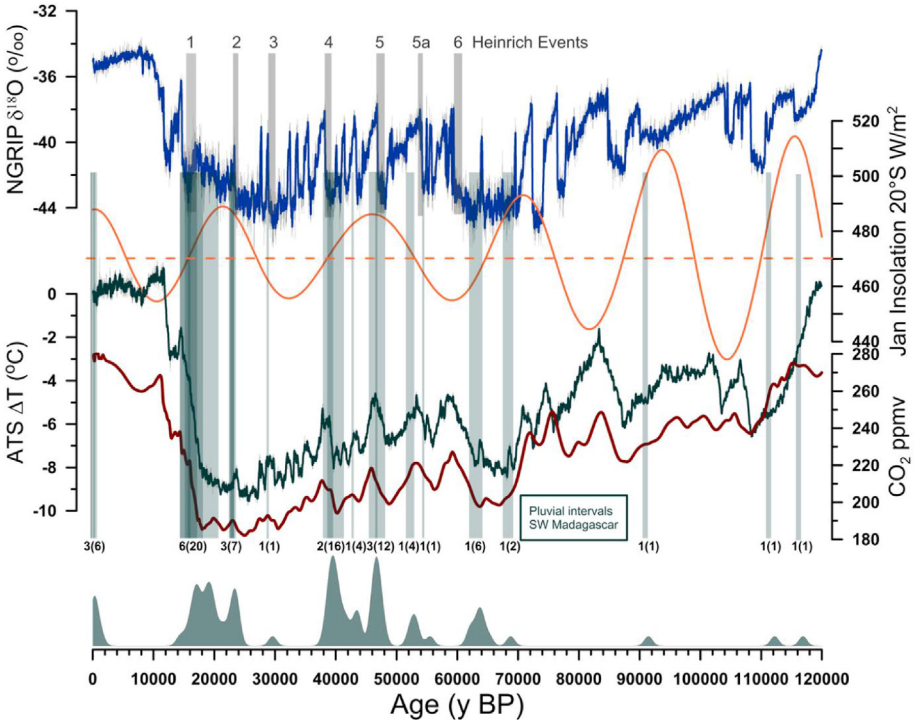

Fig. 4. Periods of speleothem growth from Southwest Madagascar over the past 120 ky, shaded green bars, are shown together with Greenland NGRIP $\delta^{18}O$ record on GICC05 × 1.0063 chronology (Andersen et al., 2004; WAIS Divide Project Members, 2015) timing of Heinrich events 1–6, time series of Antarctic temperature (Parrenin et al., 2013) and January insolation at 20°S (Berger and Loutre, 1992), and atmospheric CO_2 concentrations from Antarctic ice cores (Bereiter et al., 2015). The number below each period of speleothem deposition indicate the number of stalagmites that grew in each period and, in parentheses, the number of $^{230}Th/U$ age determinations used to define each period. At the bottom of the figure is a kernel density curve giving the age probability versus time (Sharman et al., 2018; Weij et al., 2020).

4. Discussion

4.1. Climatic controls on speleothem growth periods

Fig. 4 shows the growth periods of the 18 stalagmites together with high latitude records of climate from Antarctic and Greenland ice cores and January insolation for 20°S latitude. Our interpretation of the growth periods is that they represent periods in which there is/was sufficient rainfall for plant and soil activity to produce enough soil CO_2 to activate the karst system and allow speleothem growth. We interpret the longer periods in which we do not record stalagmite growth as having been too dry to support active deposition of speleothems. This interpretation is supported by the six samples that include multiple growth periods separated by long hiatuses. In our interpretation, the periods during which stalagmites grew indicate expansion of the southern margin of the Indian Ocean ITCZ to the south during the DJF rainy season. Periods absent stalagmites mark times when the southern margin of the ITCZ shifted to the north. For the great majority of the stalagmites, deposition seems to require the conjunction of two phenomena: summer insolation that is greater than the median of the total range in insolation values over the precession cycle and relatively warm conditions in Antarctica. During the last glacial period stalagmite growth occurred exclusively coincident with part or all of an Antarctic Isotope Maximum (AIM), the millennial-scale warm intervals in the Antarctic ice core record. Speleothem growth is not always centered on peak warmth of an AIM, with some pluvial periods occurring during the period of an AIM in which Antarctic temperatures are increasing, for example from 48 ka to 46 ka and from 41 ka to 39 ka. In addition, the glacial termination, the largest and most rapid period of increasing Antarctic temperatures is marked by a large number of speleothems. The growth intervals do not show a clear relationship to Northern Hemisphere millennial temperature variations, Heinrich events and Dansgaard/Oeschger cycles, that dominate climate variations over the last glacial period in the Northern Hemisphere and much of the tropics. Two exception to the above relationships are observed, at 29.6 ka and 55.5 ka. In each case, a few centimeters of speleothem growth took place during an AIM but also when summer insolation was below the median and coincident with deposition of Heinrich layers 3 and 5a, respectively.

On orbital timescales, our results agree well with Northern and Southern Hemisphere records of tropical rainfall that show antiphase behavior between the Northern and Southern Hemisphere tropics. Numerous paleoclimate records and modelling studies of tropical climate demonstrate that as precession of Earth's orbit changes the amount of incoming summer solar insolation, summer rainfall varies in phase with insolation, driven by the sensible and latent heat components of the monsoons (Bosmans et al., 2018; Cheng et al., 2009; Prell and Kutzbach, 1987). This orbital control on tropical rainfall results in changes in monsoon rainfall that are in phase with precession maxima in each hemisphere and, therefore, antiphase between the Northern and Southern Hemisphere tropics (Wang et al., 2014). The observed growth periods of stalagmites in southwestern Madagascar occur almost entirely when summer insolation is near or greater than the midpoint of precession-driven variations (Fig. 4). This relationship holds true for 24 of 26 different stalagmite growth periods. Only two sampled stalagmites grew when summer isolation was below the midpoint of the precession cycle.

At the millennial scale of climate variability, however, our record contrasts with many other records of the Southern Hemisphere

Table 1
Sample ages and radiogenic isotope geochemistry.

Sample ID	Depth (mm)	^{238}U (ng/g)[a]	± (2 σ)	^{232}Th (pg/g)[a]	± (2σ)	^{234}U (per mil)[b]	± (2 σ)	(^{230}Th/^{238}U) ± (2σ) activity		(^{230}Th/^{232}Th)± (2σ) ppm atomic		Age (yr)± (2σ) (uncorrected)[c]		Age (yr)± (2σ) (corrected)[d]		^{234}U$_i$ ± (2σ) (per mil)[e]		Age (yr BP) ±(2σ) (corrected)[f]	
AD - 1	13	86.7	1.7	243.5	4.89	−63.3	3.6	0.14397	0.00055	814	3	18,233	109	18,142	118	−67	4	18,076	118
AD - 1	75	74.4	1.5	171.3	3.62	−61.1	4.0	0.14934	0.00134	1030	11	18,927	207	18,853	210	−64	4	18,786	210
AD - 1	295	85.4	1.7	465.5	9.41	−58.5	2.1	0.15909	0.00112	464	3	20,223	164	20,047	186	−62	2	19,981	186
AD - 1	540	65.7	1.3	1015.0	20.34	−62.9	1.9	0.17121	0.00092	176	1	22,049	142	21,548	288	−67	2	21,481	288
AD - 1	559	104.7	2.1	61.4	1.76	−64.0	1.9	0.15583	0.00092	4220	90	19,899	137	19,880	137	−68	2	19,814	137
AD - 2	17	99.0	2.0	40.5	1.32	−107.1	2.3	0.26302	0.00150	10,203	269	38,343	293	38,329	293	−119	3	38,262	293
AD - 2	31	110.3	2.2	12.1	0.32	−103.5	1.9	0.26825	0.00133	38,758	677	39,064	259	39,060	259	−116	2	38,990	259
AD - 2	107	70.0	1.4	30.9	1.32	−105.3	2.5	0.26840	0.00121	9666	369	39,189	255	39,174	255	−118	3	39,105	255
AD - 2	111	77.1	1.5	56.0	1.14	−103.3	1.8	0.26917	0.00132	5885	35	39,212	255	39,188	255	−115	2	39,117	255
AD - 2	203	96.5	1.9	8.1	0.21	−107.3	2.0	0.27431	0.00110	51,849	841	40,362	230	40,359	230	−120	2	40,289	230
AD - 2	214	132.2	2.6	16.0	1.37	−103.9	3.4	0.27190	0.00154	35,660	2973	39,729	337	39,725	337	−116	4	39,659	337
AD - 2	296	95.5	1.9	26.6	0.57	−111.3	2.0	0.27180	0.00138	15,506	138	40,139	274	40,130	274	−125	2	40,060	274
AD - 2	305	111.1	2.2	101.6	2.48	−108.6	1.9	0.28125	0.00092	4881	69	41,690	203	41,659	203	−122	2	41,592	203
AD - 2	348	88.2	1.8	19.8	0.83	−109.1	1.8	0.27132	0.00105	19,210	713	39,928	215	39,921	215	−122	2	39,854	215
AD - 2	350	104.2	2.1	11.6	0.30	−108.2	2.0	0.27245	0.00110	38,701	641	40,080	229	40,076	229	−121	2	40,006	229
AD - 2	366	108.0	2.2	83.6	1.93	−104.4	4.8	0.26922	0.00098	5518	64	39,286	320	39,260	320	−117	5	39,191	320
AD - 3	5	67.0	1.3	141.6	3.04	−103.0	2.0	0.29444	0.00120	2211	19	43,753	254	43,681	257	−116	2	43,612	257
AD - 3	12.5	63.6	1.3	279.5	5.64	−90.1	2.2	0.29977	0.00142	1083	6	43,905	294	43,757	303	−102	2	43,687	303
AD - 3	26	54.5	1.1	752.5	15.16	−92.8	2.4	0.30020	0.00172	345	2	44,158	351	43,690	421	−105	3	43,620	421
AD - 3	28	56.2	1.1	896.9	18.03	−84.2	3.6	0.29981	0.00129	298	1	43,539	321	43,004	417	−95	4	42,936	417
AD - 3	36	57.0	1.1	46.6	1.11	−81.6	2.0	0.31490	0.00123	6108	83	46,110	261	46,083	262	−93	2	46,017	262
AD - 3	46	68.2	1.4	144.7	2.93	−75.8	2.3	0.31702	0.00164	2372	14	46,104	337	46,034	339	−86	3	45,964	339
AD - 3	178	61.2	1.2	394.3	7.94	−75.2	1.9	0.32105	0.00193	791	5	46,802	376	46,589	391	−86	2	46,519	391
AD - 3	201	68.7	1.4	891.0	17.94	−84.2	2.8	0.31787	0.00148	389	2	46,834	337	46,400	400	−96	3	46,331	400
AD - 3	366	41.8	0.8	518.3	10.45	−73.4	2.2	0.32400	0.00225	414	3	47,219	438	46,808	484	−84	2	46,738	484
AD - 3	370	45.0	0.9	127.9	2.66	−71.3	3.0	0.22224	0.00136	1242	10	29,934	242	29,841	246	−78	3	29,775*246	
AD - 3	386	40.5	0.8	142.1	3.05	−71.0	2.1	0.32332	0.00146	1465	13	46,933	301	46,817	307	−81	2	46,749	307
AD - 4	20.5	88.9	1.8	204.3	4.16	−107.5	1.4	0.11931	0.00095	824	7	15,692	137	15,614	143	−112	1	15,549	143
AD - 4	74	64.8	1.3	85.0	2.19	−107.1	2.9	0.12468	0.00084	1508	26	16,449	134	16,418	135	−112	3	16,350	135
AD - 4	113.5	58.3	1.2	76.7	1.71	−134.0	2.3	0.12374	0.00087	1494	18	16,880	138	16,834	140	−141	2	16,769	140
AD - 4	168	55.5	1.1	119.5	2.53	−137.4	2.6	0.12848	0.00069	948	8	17,662	119	17,586	125	−144	3	17,521	125
AD - 4	201.5	49.3	1.0	84.1	2.14	−126.4	2.4	0.12946	0.00111	1205	21	17,557	172	17,517	174	−133	2	17,448	174
AD - 4	234.5	112.9	2.3	285.3	5.78	−142.4	2.9	0.13521	0.00090	850	6	18,797	155	18,707	161	−150	3	18,642	161
AD - 4	301.5	143.4	2.9	705.4	14.15	−144.4	2.3	0.13746	0.00055	444	2	19,194	103	19,018	135	−152	2	18,953	135
AD - 4	311.5	110.2	2.2	423.9	8.63	−146.9	2.3	0.13832	0.00078	571	4	19,388	134	19,294	142	−155	2	19,225	142
AD - 4	351	82.3	1.6	82.7	1.81	−148.5	1.8	0.20158	0.00086	3188	31	29,702	167	29,666	168	−161	2	29,600	168
AD - 5	39	246.8	4.9	506.1	10.35	−161.0	2.7	0.00156	0.00006	12	0	203	8	129	38	−161	3	60	38
AD - 5	77	345.9	6.9	390.9	7.98	−166.4	2.0	0.00315	0.00004	44	1	414	6	373	21	−167	2	303	21
AD - 5	121	433.6	8.7	401.3	8.22	−152.6	2.0	0.00342	0.00005	59	1	441	6	408	18	−153	2	338	18
AD - 5	146	454.5	9.1	2365.4	47.79	−145.1	1.9	0.00416	0.00013	13	0	532	17	348	94	−145	2	279	94
AD - 7	146	312.3	6.2	146.0	3.20	−114.5	1.9	0.00330	0.00007	112	2	407	8	391	12	−115	2	322	12
AD - 9	8	49.7	1.0	61.4	1.58	−120.5	2.5	0.26229	0.00165	3375	58	38,959	329	38,916	329	−134	3	38,847	330
AD - 9	18.5	53.4	1.1	16.3	0.43	−122.3	2.9	0.26488	0.00150	13,782	245	39,535	320	39,524	320	−137	3	39,454	320
AD - 9	152	75.7	1.5	65.2	1.36	−110.7	2.0	0.27399	0.00145	5050	40	40,504	288	40,474	288	−124	2	40,404	289
AD - 9	252	72.3	1.4	16.1	0.43	−105.6	1.8	0.27993	0.00130	19,895	360	41,267	258	41,259	258	−119	2	41,189	258
AD - 9	272.5	87.3	1.7	1383	27.73	−99.2	2.7	0.28869	0.00122	289	1	42,463	278	41,922	387	−112	3	41,854	387
AD - 9	290	70.2	1.4	9.3	0.37	−16.1	1.8	0.64571	0.00241	77,109	2657	116,968,902	116,964,902	−22	3 116,890 4902				
AD - 10	5	176.8	3.5	14.3	1.09	−227.9	2.2	0.11112	0.00065	21,862	1613	17,075	122	17,072	122	−239	2	17,003	122
AD - 10	218	316.3	6.3	16.1	1.03	−229.3	1.8	0.13535	0.00053	42,319	2573	21,267	110	21,265	110	−243	2	21,196	110
AD - 11	11	48.7	1.0	92.2	1.89	−72.2	3.4	0.32159	0.00167	2696	18	46,700	383	46,638	384	−82	4	46,568	384
AD - 11	22	51.7	1.0	289.2	5.83	−69.3	1.9	0.32369	0.00195	918	6	46,884	378	46,700	389	−79	2	46,630	389
AD - 11	51.5	52.8	1.1	25.8	0.83	−69.9	3.0	0.32628	0.00201	10,623	273	47,400	420	47,384	420	−80	3	47,314	420
AD - 11	74	67.3	1.3	175.9	3.55	−75.1	2.6	0.31615	0.00179	1921	12	45,901	370	45,814	372	−85	3	45,744*372	
AD - 11	282.5	60.6	1.2	11.9	0.34	−73.0	1.7	0.32475	0.00145	26,232	531	47,329	291	47,322	291	−83	2	47,252	292

AD - 11	568	46.1	0.9	9.1	0.43	−69.8	3.1	0.32955	0.00171	26,395	1133	47,988	383	47,982	383	−80	4	47,912	383
AY - 1	14	46.1	0.9	4052.5	81.27	−3.8	2.9	0.57607	0.00255	104	0	94,215	823	91,514	1593	−5	4	91,446	1593
AY - 1	239	50.4	1.0	38.6	1.41	−35.4	3.2	0.61693	0.00225	12,796	395	1,123,101,053	1,122,851,053	−49	4	112,217 1053			
AY - 2	212	102.2	2.0	2313.7	46.53	−11.0	1.9	0.35166	0.00146	247	1	47,956	278	47,260	445	−13	2	47,192	445
F - 1	9	183.2	3.7	7623.6	152.72	−41.5	1.5	0.02382	0.00068	9	0	2745	80	1424	669	−42	2	1357	669
F - 1	80	261.8	5.2	2452.5	49.47	−37.8	2.7	0.15765	0.00069	267	1	19,536	113	19,241	186	−40	3	19,172	186
F - 1	187	277.7	5.6	2102.0	42.24	−39.9	1.4	0.18531	0.00068	389	2	23,418	103	23,179	158	−43	1	23,112	158
F - 3	53	235.4	4.7	12,078	244.20	−61.2	2.3	0.42842	0.00217	133	1	67,001	535	65,313	1003	−74	3	65,243	1003
F - 3	179	203.6	4.1	1115.2	22.58	−56.7	3.4	0.43997	0.00186	1275	6	69,031	560	68,853	566	−69	4	68,783	566
MT - 2	5	150.3	3.0	12.1	1.06	−103.0	2.8	0.12674	0.00062	24,948	2118	16,659	105	16,656	105	−108	3	16,587	105
MT - 2	462	163.8	3.3	26.2	1.23	−102.9	2.0	0.13085	0.00074	13,001	558	17,244	114	17,238	114	−108	2	17,170	114
MT - 3	33	331.8	6.6	435.8	8.88	−93.9	2.6	0.34263	0.00156	4142	24	52,295	372	52,251	372	−109	3	52,181	372
MT - 3	70	321.5	6.4	1324.4	26.78	−105.3	1.6	0.30118	0.00148	1161	6	45,158	297	45,017	305	−120	2	44,947*305	
MT - 3	159	356.2	7.1	279.6	5.68	−119.2	1.6	0.26317	0.00098	5323	26	39,045	197	39,017	198	−133	2	38,947*198	
MT - 3	177	325.9	6.5	828.1	16.70	−91.4	2.6	0.34619	0.00146	2163	10	52,797	360	52,711	362	−106	3	52,642	362
MT - 3	192	299.8	6.0	395.6	8.03	−90.0	1.9	0.34976	0.00190	4208	26	53,391	408	53,347	409	−105	2	53,277	409
MT - 3	283	290.2	5.8	210.5	4.31	−90.4	1.5	0.34873	0.00145	7633	44	53,213	314	53,188	314	−105	2	53,119	314
MT - 3	295	306.7	6.1	415.0	8.48	−91.4	2.1	0.36027	0.00136	4227	23	55,621	330	55,576	330	−107	2	55,506	331
MT - 3	361	733.5	14.7	883.1	17.76	−134.7	3.5	0.22328	0.00078	2944	10	32,816	214	32,774	215	−148	4	32,704*215	
MT - 3	391	406.7	8.1	152.8	3.16	−70.6	1.5	0.40106	0.00151	16,946	105	62,122	351	62,109	351	−84	2	62,040	351
MT - 3	433	335.6	6.7	157.3	3.26	−70.8	2.4	0.40774	0.00192	13,814	96	63,556	477	63,541	477	−85	3	63,471	477
MT - 3	451	308.0	6.2	367.0	7.58	−71.9	2.5	0.40920	0.00134	5453	32	63,985	384	63,945	385	−86	3	63,876	385
MT - 3	456	249.1	5.0	232.6	4.75	−71.8	1.8	0.41002	0.00159	6973	38	64,148	390	64,117	391	−86	2	64,047	391
MT - 3	480	308.3	6.2	234.3	4.80	−69.5	1.7	0.40914	0.00163	8549	48	63,727	387	63,702	388	−83	2	63,632	388
MT - 3	515	297.8	6.0	256.6	5.26	−70.5	2.2	0.40265	0.00103	7420	36	62,441	310	62,413	310	−84	3	62,344	310
MT - 4	16	185.0	3.7	811.5	16.28	−141.6	2.6	0.10723	0.00052	388	2	14,605	90	14,449	119	−148	3	14,380	119
MT - 4	621	161.9	3.2	20,338	407.29	−143.9	2.4	0.17111	0.00288	22	0	24,472	472	19,895	2381	−152	3	19,827	2381
SR - 1	23	76.2	1.5	490.1	9.94	−260.9	1.8	0.13859	0.00144	342	4	22,932	276	22,662	307	−278	2	22,592	307
SR - 1	240	69.2	1.4	806.9	16.21	−309.2	1.6	0.13230	0.00092	180	1	23,569	197	23,042	329	−330	2	22,971	329
SR - 1	422	89.3	1.8	1279.8	25.71	−343.9	1.7	0.12925	0.00066	143	1	24,410	162	23,723	380	−368	2	23,652	380
SR - 2	197	72.3	1.4	28.7	0.64	−107.0	2.5	0.17392	0.00083	6942	75	23,725	149	23,711	150	−114	3	23,641	150
SR - 2	217	68.6	1.4	68.0	1.38	−106.4	2.5	0.17371	0.00084	2783	16	23,675	149	23,641	150	−114	3	23,571	150
SR - 2	254	83.8	1.7	90.5	1.83	−104.8	2.0	0.17488	0.00104	2572	17	23,804	171	23,767	172	−112	2	23,697	172

Notes.

* These samples are significant are outliers and thought to be altered post-deposition. They were not used in constructing Figs. 4 and 5.

[a] Reported errors for ^{238}U and ^{232}Th concentrations are estimated to be ±1% due to uncertainties in spike concentration; analytical uncertainties are smaller.

[b] $\delta^{234}U = ([^{234}U/^{238}U]_{activity} - 1) \times 1000$.

[c] $[^{230}Th/^{238}U]_{activity} = 1 - e^{-\lambda 230 T} + (\delta^{234}U_{measured}/1000)[\lambda_{230}/(\lambda_{230} - \lambda_{234})](1 - e^{-(\lambda 230 - \lambda 234) T})$, where T is the age. "Uncorrected" indicates that no correction has been made for initial ^{230}Th.

[d] Ages are corrected for detrital ^{230}Th assuming an initial $^{230}Th/^{232}Th$ of $(4.4 \pm 2.2) \times 10^{-6}$.

[e] $\delta^{234}U_{initial}$ corrected was calculated based on ^{230}Th age (T), i.e., $\delta^{234}U_{initial} = \delta^{234}U_{measured} X e^{\lambda 234 * T}$, and T is corrected age.

[f] B.P. stands for "Before Present" where the "Present" is defined as the January 1, 1950 C.E. Decay constants for ^{230}Th and ^{234}U are from Cheng et al. (2013); decay constant for ^{238}U is 1.55125×10^{-10} yr^{-1} (Jaffey et al., 1971).

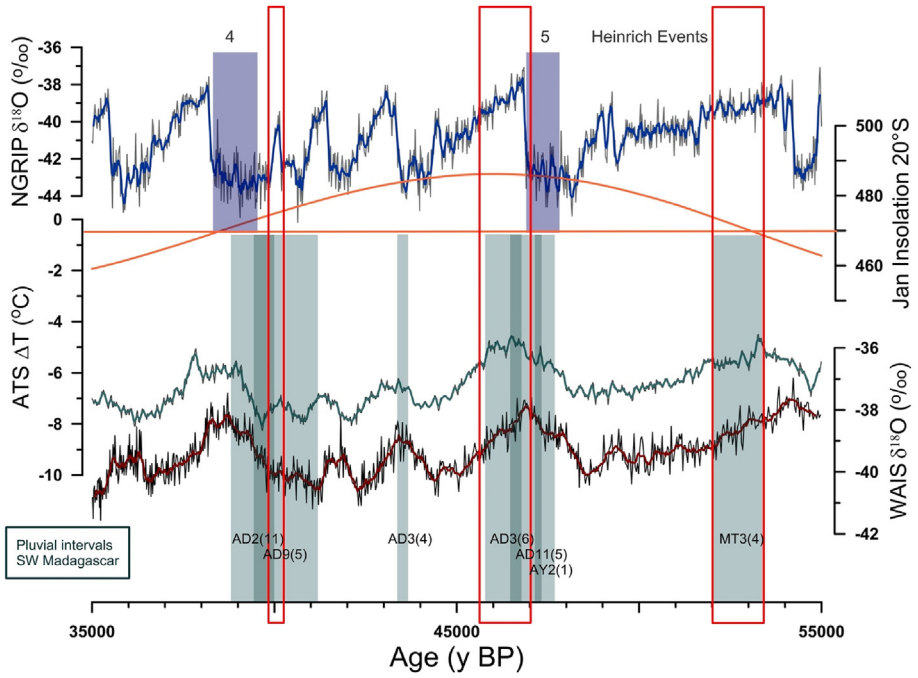

Fig. 5. Detailed record of periods of deposition of stalagmites from southwest Madagascar from 55 ky BP to 35 ky BP. Here, the NGRIP $\delta^{18}O$ and insolation as above are shown with two separate Antarctic temperature records, the ATS as above and WAIS divide ice core $\delta^{18}O$ (WAIS Divide Project Members, 2015), each on its own timescale. Individual speleothems are designated with the number of $^{230}Th/U$ age determinations for each in parentheses. The red rectangles highlight examples of periods of ITCZ expansion in both hemispheres.

component of the ITCZ, particularly during the last glacial period (Kanner et al., 2012; Wang et al., 2004). Increased rainfall in the study area, which we interpret as extensions of the southern margin of the rainfall belt, are all coincident with millennial periods of warmth in Antarctica. Some of the periods of stalagmite growth in the study area do overlap with Heinrich or Greenland stadial intervals. Close examination of the growth periods, however, reveals that growth often continues well beyond the termination of Heinrich events and beyond the transition from stadial to interstadial portions of D/O cycles (Fig. 5). In one case, from 55 ky BP to 53 ky BP, growth occurred wholly during a D/O interstadial and entirely unassociated with a Heinrich event (Fig. 5). Our interpretation is that in the Southern Indian Ocean region the southern margin of the tropical rainfall belt responds almost wholly to Southern Hemisphere insolation and temperature and independently of the climate of the high northern latitudes. At the millennial scale, warmth in the high southern latitudes extends the margin of the tropics to the south during AIM, rather than changes in the mean ITCZ latitude driven by Northern Hemisphere temperature.

4.2. Northern vs Southern Hemisphere forcing

In prior studies of Southern Hemisphere climate at sub-orbital timescales during the last glacial period, increases in tropical rainfall are observed to coincide with stadial (cold). portions of D/O cycles, an effect particularly pronounced for stadials associated with Heinrich events (Burns et al., 2003; Kanner et al., 2012; Stríkis et al., 2018; Wang et al., 2004). Our results indicate that for the monsoon systems surrounding the Indian Ocean there is also an antiphase response between the two hemispheres to Southern Hemisphere millennial-scale temperature change during the last glacial period. Warm high southern latitude temperatures expand the southern boundary of the Indian Ocean monsoon, while they decrease the intensity of Northern Hemisphere monsoons in India and Asia (Cai et al., 2006; Chen et al., 2016; Rohling et al., 2009).

Our record may differ from the great majority of previous studies because it may record migration of the southern margin the ITCZ, not the overall intensity of tropical summer rainfall. Alternatively, there may be regional differences in the sensitivity of Southern Hemisphere tropical rainfall to Northern as opposed to Southern Hemisphere temperatures (Atwood et al., 2020). Monsoon rainfall in Madagascar is strongly correlated to western Indian Ocean tropical sea surface temperatures (SST) in modern (Koseki and Bhatt, 2018) and paleoclimate records (Tierney et al., 2008; Weldeab et al., 2014). This observed relationship offers a mechanistic explanation for the observed pattern of wet periods in the study area. Tropical Indian Ocean SSTs during the last glacial period are themselves correlated with AIM, with 1–2 °C of SST warming during AIM events (Kiefer et al., 2006). Increases in SSTs during AIM should increase the latent heat component of the monsoon leading to increased rainfall in the study area, at least during the phases in the precession cycle that provide sufficient sensible heating to intensify the Southern Hemisphere monsoon in general.

4.3. Expansion and contraction of the tropical rainfall belt

Our results also have implications for the behavior of the tropical rainfall belt in general. Fig. 5 shows that from 48 ky BP to 46 ky BP, the period covering Heinrich event 5, D/O cycle 12 and corresponding AIM 12, stalagmite growth in the study area overlaps the stadial/interstadial transition in Greenland temperatures. That transition is seen in the Northern Hemisphere tropics as an intensification in the East Asian and Indian monsoons and is often interpreted as indicating a northward shift in the ITCZ at that time. Our record shows that the southern limit of the ITCZ does not shift northward at that time but does so approximately 1000 years later.

For that 1000 years, the sudden warming at high northern latitudes draws the northern limit of the ITCZ north, but continued warmth in the high southern latitudes maintains an extension of the southern limit of the ITCZ far to the south. Another example is the growth of stalagmite MT-3 from 53.5 ky BP to 52 ky BP. Increasing summer solar insolation combines with relatively high temperatures at high southern latitudes to increase rainfall at the southern edge of the tropics. That time period overlaps with the peak warmth of D/O interstadial 14, also a period of increased Northern Hemisphere monsoon intensity. Thus, our data indicate that the ITCZ can simultaneously expand both north and south, broadening the overall extent of the ITCZ. The southern limit of the ITCZ moves north only after the high southern latitudes gradually cool. Indeed, contraction of the southern limit of the ITCZ occurs as the NH monsoons weaken, suggesting that the ITCZ is simultaneously contracting in both hemispheres. These results suggest that our paradigm of antiphase behavior of rainfall in the Northern vs Southern Hemisphere tropics in response to migration in the zonal mean ITCZ has exceptions. When the high latitudes warm or cool simultaneously, the width of the ITCZ can expand or contract in response. Expansion and contraction of the ITCZ in response to orbital forcing is seen in the results of some climate models (Singarayer et al., 2017), but the phenomenon has not been well documented in the paleoclimate record of the last glacial.

4.4. Relationship between rainfall and atmospheric pCO_2

The warm AIM recognized during the last glacial period are also associated with periods of higher atmospheric CO_2 concentrations (Ahn and Brook, 2008). Therefore, the periods of an expanded ITCZ observed in our results may also provide a paleoclimate perspective into the response of tropical hydrology to warming associated with anthropogenic greenhouse gas forcing. Currently, modelling results of the response of the ITCZ to anthropogenic global warming vary widely, with some suggesting that the ITCZ will narrow, while others suggest that it will broaden(Byrne et al., 2018). A majority of models, however, suggest a narrowing of the ITCZ, weakening and broadening of the Hadley circulation, and drying of the subtropics and edges of the tropics in response to greenhouse gas forcing (Byrne et al., 2018; Lau and Kim, 2015). Most models also show greater tropical expansion in the Southern Hemisphere (Yang et al., 2020) Direct observations support expansion of the tropics through widening of the Hadley circulation, particularly in the Southern Hemisphere (Grise et al., 2019), but do not address whether the rainfall belt also expands as the tropics widen. A complete review of the voluminous literature associated with predicting the response of tropical rainfall to greenhouse gas forcing is beyond the scope of this paper. And while the model consensus seems to imply that the above synopsis is robust, it should be noted that model results vary widely, are complicated by uncertainty in the response of precipitation to atmospheric aerosols, non-uniform SST changes, Walker circulation changes and the impact of possible changes in the meridional overturning current. The subject remains, of course, an area of intense research.

Our results do not align with the majority of model results. Within the periods of sufficient summer solar insolation, we find that the southern limit of the ITCZ expands southward in response to increased Southern Hemisphere temperatures and atmospheric CO_2. For some time periods, the southward expansion overlaps interstadial parts of D/O events, which are interpreted as indicating a more northerly position of the ITCZ. However, when atmospheric warmth in the high northern and southern latitudes coincides, as is projected to be the response to AGW, our data indicate expansion of the rainfall belt on both sides of the equator. On timescales of the next few hundred years, summer insolation in the Southern Hemisphere will remain near its peak and essentially constant as a forcing mechanism. As AGW proceeds, both hemispheres will warm with amplified warming at the poles (IPCC et al., 2013). Our paleoclimate results suggest that, in response to that warming, the southern edge of the ITCZ in the Indian Ocean should expand to the south. Recent climate model results that focus on the Southern Hemisphere tropics support this inference (Pascale et al., 2019; D'Agostino et al., 2020). Thus, while it is possible that the western Indian Ocean region is anomalous with respect to other areas of the tropics (Atwood et al., 2020), being more strongly influenced by local tropical SSTs as discussed above, it may also be representative of other parts of the Southern Hemisphere. Further research on past changes in the southern margins of the ITCZ in other areas is needed to clarify past and future changes in rainfall on the southern margin of the tropics and to provide a paleoclimate perspective on the controls on ITCZ width.

Funding sources

This research was supported by the National Science Foundation grants AGS-1702891/1702691 and BCS-1750598.

Author contributions

S.J.B and L.R.G. conceived the research project. S.J. Burns wrote the manuscript. D.M, C.W.K. and N.S. made the age determinations. S.J.B., L.R.G., N.S., P.F. and L.R. carried out the field work and sampling. All authors contributed to editing the manuscript.

Declaration of competing interest

The authors declare no competing interests.

Acknowledgements

We are extremely grateful to Madagascar National Parks for their cooperation and support during field work and for permission to sample from Tsimanampesotse National Park. Underwater operations were coordinated by Zachary Klukkert, Phillip Lehman, Ryan Dart and Patrick Widman, and carried out by Klukkert and divers from the Madagascar Cave Diving Association (MCDA), the Dominican Republic Speleological Society (DRSS), and ProTec Dive Centers with critical logistical support from the Anakao Ocean Lodge. Field research was conducted under a collaborative accord between the University of Antananarivo (Mention Bassins sédimentaires, Evolution, Conservation) and the University of Massachusetts Amherst (Departments of Anthropology and Geosciences). We are also grateful for the support and cooperation of the Ministère de la Communication et de la Culture for permission to conduct field work and recover and export samples, and to the Ministère auprès de la Présidence Chargé des Mines et du Pétrole, for permission to sample and export material to the U.S.A. We thank Adam Jost and Benjamin Hardt for assisting with U/Th analyses at MIT. We thank two anonymous reviewers for their very helpful comments.

Appendix 1. Age depth plots and photographs of all stalagmites analyzed. Age determination shown in red are outliers not used in results or discussion

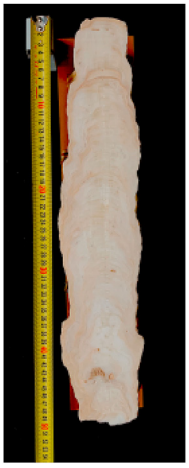

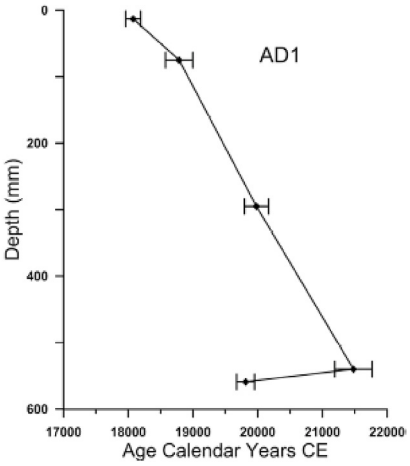

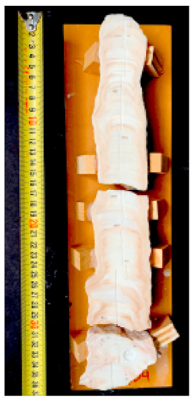

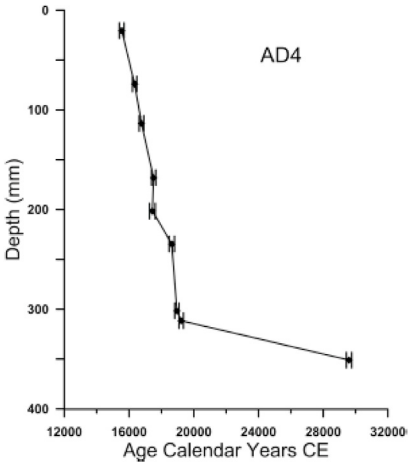

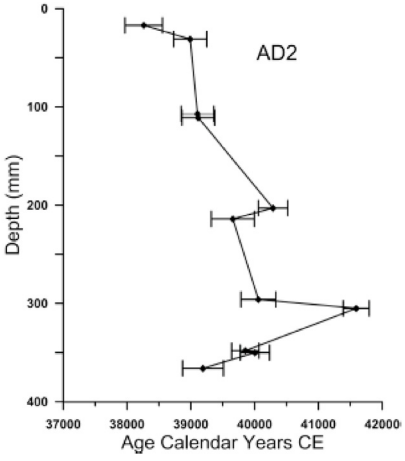

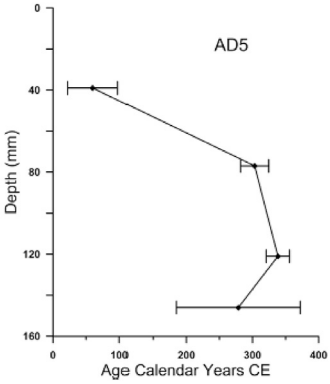

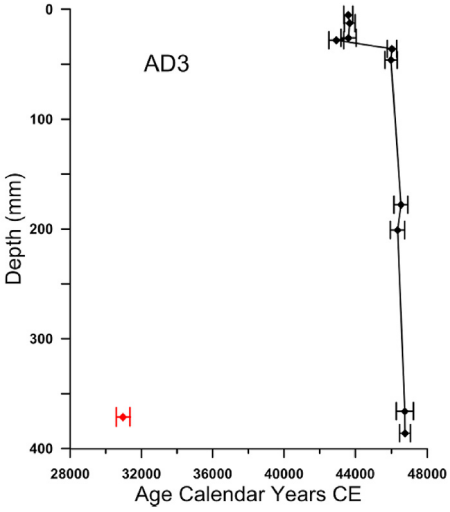

AD7

322 +/- 12

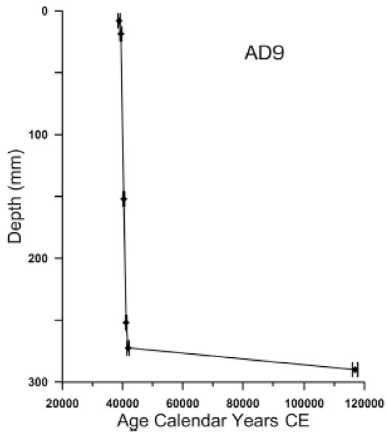

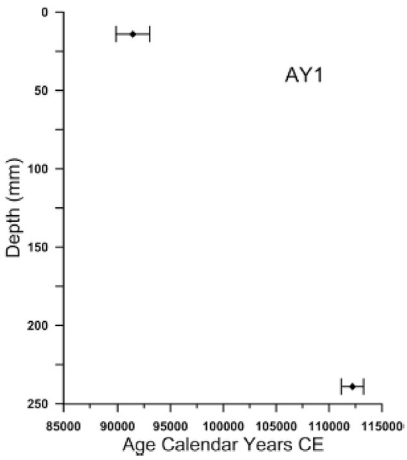

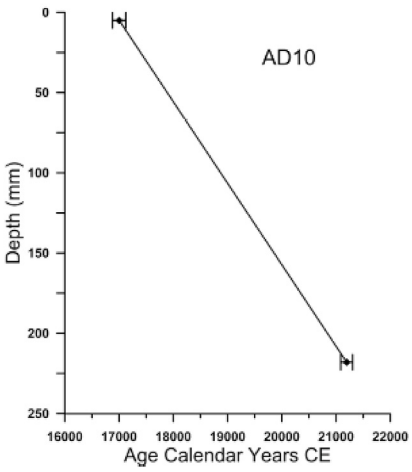

AY2

47192 +/- 445

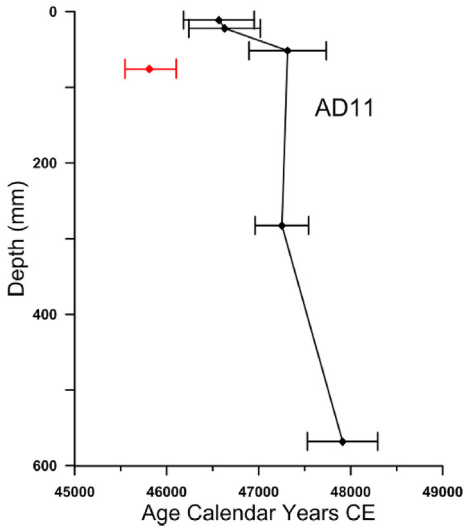

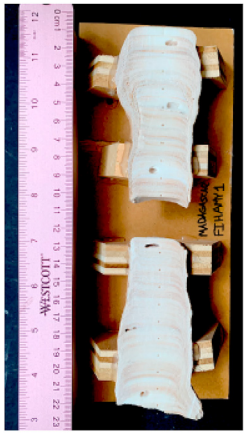

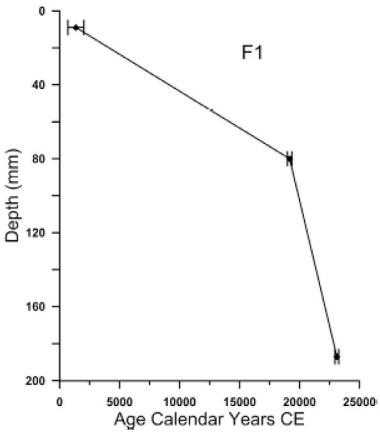

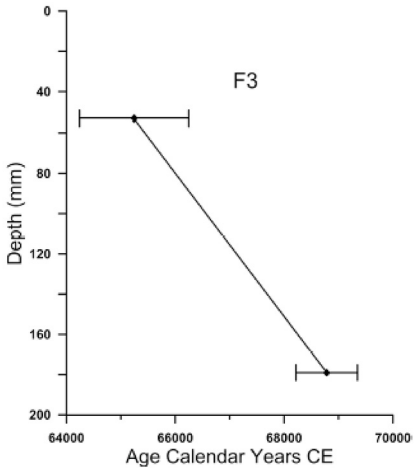

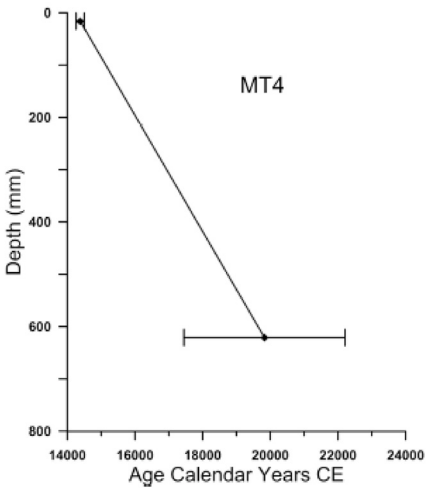

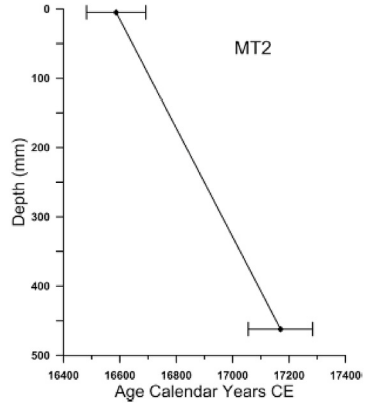

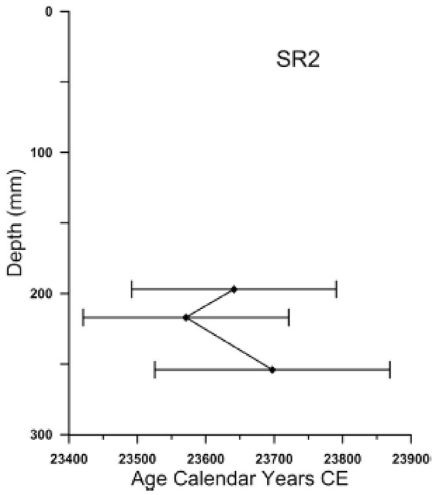

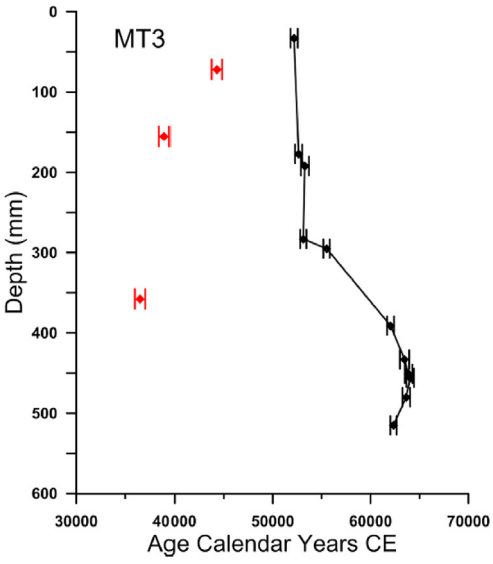

References

Ahn, J., Brook, E.J., 2008. Atmospheric CO2 and climate on millennial time scales during the last glacial period. Science 322, 83–85. https://doi.org/10.1126/science.1160832.

Andersen, K.K., Azuma, N., Barnola, J.-M., Bigler, M., Biscaye, P., Caillon, N., Chappellaz, J., Clausen, H.B., Dahl-Jensen, D., Fischer, H., Flückiger, J., Fritzsche, D., Fujii, Y., Goto-Azuma, K., Grønvold, K., Gundestrup, N.S., Hansson, M., Huber, C., Hvidberg, C.S., Johnsen, S.J., Jonsell, U., Jouzel, J., Kipfstuhl, S., Landais, A., Leuenberger, M., Lorrain, R., Masson-Delmotte, V., Miller, H., Motoyama, H., Narita, H., Popp, T., Rasmussen, S.O., Raynaud, D., Rothlisberger, R., Ruth, U., Samyn, D., Schwander, J., Shoji, H., Siggard-Andersen, M.-L., Steffensen, J.P., Stocker, T., Sveinbjörnsdóttir, A.E., Svensson, A., Takata, M., Tison, J.-L., Thorsteinsson, Th, Watanabe, O., Wilhelms, F., White, J.W.C., North Greenland Ice Core Project members, 2004. High-resolution record of Northern Hemisphere climate extending into the last interglacial period. Nature 431, 147–151. https://doi.org/10.1038/nature02805.

Atwood, A.R., Donohoe, A., Battisti, D.S., Liu, X., Pausata, F.S.R., 2020. Robust longitudinally variable responses of the ITCZ to a myriad of climate forcings. Geophys. Res. Lett. 47, e2020GL088833. https://doi.org/10.1029/2020GL088833.

Bereiter, B., Eggleston, S., Schmitt, J., Nehrbass-Ahles, C., Stocker, T.F., Fischer, H., Kipfstuhl, S., Chappellaz, J., 2015. Revision of the EPICA Dome C CO2 record from 800 to 600 kyr before present. Geophys. Res. Lett. 42, 542–549. https://doi.org/10.1002/2014GL061957.

Berger, A., Loutre, M.F., 1992. Astronomical solutions for paleoclimate studies over the last 3 million years. Earth Planet Sci. Lett. 111, 369–382. https://doi.org/

10.1016/0012-821X(92)90190-7.
Bosmans, J.H.C., Erb, M.P., Dolan, A.M., Drijfhout, S.S., Tuenter, E., Hilgen, F.J., Edge, D., Pope, J.O., Lourens, L.J., 2018. Response of the Asian summer monsoons to idealized precession and obliquity forcing in a set of GCMs. Quat. Sci. Rev. 188, 121–135. https://doi.org/10.1016/j.quascirev.2018.03.025.
Brown, E.T., Johnson, T.C., Scholz, C.A., Cohen, A.S., King, J.W., 2007. Abrupt change in tropical African climate linked to the bipolar seesaw over the past 55,000 years. Geophys. Res. Lett. 34. https://doi.org/10.1029/2007GL031240.
Burney, D.A., 1987. Late Holocene vegetational change in central Madagascar. Quat. Res. 28, 130–143. https://doi.org/10.1016/0033-5894(87)90038-X.
Burney, D.A., 1993. Late Holocene environmental changes in arid southwestern Madagascar. Quat. Res. 40, 98–106. https://doi.org/10.1006/qres.1993.1060.
Burns, S.J., Fleitmann, D., Matter, A., Kramers, J., Al-Subbary, A.A., 2003. Indian Ocean climate and an absolute chronology over Dansgaard/Oeschger events 9 to 13. Science 301, 1365–1367.
Burns, S.J., Godfrey, L.R., Faina, P., McGee, D., Hardt, B., Ranivoharimanana, L., Randrianasy, J., 2016. Rapid human-induced landscape transformation in Madagascar at the end of the first millennium of the Common Era. Quat. Sci. Rev. 134, 92–99. https://doi.org/10.1016/j.quascirev.2016.01.007.
Byrne, M.P., Pendergrass, A.G., Rapp, A.D., Wodzicki, K.R., 2018. Response of the intertropical convergence zone to climate change: location, width, and strength. Curr. Clim. Change Rep. 4, 355–370. https://doi.org/10.1007/s40641-018-0110-5.
Cai, Y., An, Z., Cheng, H., Edwards, R.L., Kelly, M.J., Liu, W., Wang, X., Shen, C.C., 2006. High-resolution absolute-dated Indian Monsoon record between 53 and 36 ka from Xiaobailong Cave, southwestern China. Geology 34, 621–624.
Castañeda, I.S., Werne, J.P., Johnson, T.C., Filley, T.R., 2009. Late Quaternary vegetation history of southeast Africa: the molecular isotopic record from Lake Malawi. Palaeogeogr. Palaeoclimatol. Palaeoecol. 275, 100–112. https://doi.org/10.1016/j.palaeo.2009.02.008.
Chen, S., Wang, Y., Cheng, H., Edwards, R.L., Wang, X., Kong, X., Liu, D., 2016. Strong coupling of Asian Monsoon and Antarctic climates on sub-orbital timescales. Sci. Rep. 6, 32995. https://doi.org/10.1038/srep32995.
Cheng, H., Edwards, R.L., Broecker, W.S., Denton, G.H., Kong, X., Wang, Y., Zhang, R., Wang, X., 2009. Ice age terminations. Science 326, 248–252. https://doi.org/10.1126/science.1177840.
Cheng, H., Sinha, A., Wang, X., Cruz, F.W., Edwards, R.L., 2012. The global paleomonsoon as seen through speleothem records from Asia and the Americas. Clim. Dynam. 39, 1045–1062. https://doi.org/10.1007/s00382-012-1363-7.
Cheng, H., Lawrence Edwards, R., Shen, C.C., Polyak, V.J., Asmerom, Y., Woodhead, J., Hellstrom, J., Wang, Y., Kong, X., Spötl, C., Wang, J., Calvin Alexander Jr, E., 2013. Improvements in 230Th dating, 230Th and 234U half-life values, and U–Th isotopic measurements by multi-collector inductively coupled plasma mass spectrometry. Earth Planet. Sci. Lett 371–372, 82–91. https://doi.org/10.1016/j.epsl.2013.04.006.
Cheng, H., Edwards, R.L., Sinha, A., Spötl, C., Yi, L., Chen, S., Kelly, M., Kathayat, G., Wang, X., Li, X., Kong, X., Wang, Y., Ning, Y., Zhang, H., 2016. The Asian monsoon over the past 640,000 years and ice age terminations. Nature 534, 640–646. https://doi.org/10.1038/nature18591.
Cruz, F.W., Burns, S.J., Karmann, I., Sharp, W.D., Vuille, M., Cardoso, A.O., Ferrari, J.A., Dias, P.L.S., Viana, O., 2005. Insolation-driven changes in atmospheric circulation over the past 116,000 years in subtropical Brazil. Nature 434, 63–66.
Duan, P., Li, H., Sinha, A., Voarintsoa, N.R.G., Kathayat, G., Hu, P., Zhang, H., Ning, Y., Cheng, H., 2021. The timing and structure of the 8.2 ka event revealed through high-resolution speleothem records from northwestern Madagascar. Quat. Sci. Rev. 268, 107104. https://doi.org/10.1016/j.quascirev.2021.107104.
D'Agostino, R., Brown, J.R., Moise, A., Nguyen, H., Silva Dias, P.L., Jungclaus, J., 2020. Contrasting southern hemisphere monsoon response: MidHolocene orbital forcing versus future greenhouse gas–induced global warming. J. Clim. 33, 9595–9613. https://doi.org/10.1175/JCLI-D-19-0672.1.
Fairchild, I., Smith, C., Baker, A., Fuller, L., Spotl, C., Mattey, D., McDermott, F., EIMP, 2006. Modification and preservation of environmental signals in speleothems. Earth Sci. Rev. 75, 105–153. https://doi.org/10.1016/j.earscirev.2005.08.003.
Fankhauser, A., McDermott, F., Fleitmann, D., 2016. Episodic speleothem deposition tracks the terrestrial impact of millennial-scale last glacial climate variability in SW Ireland. Quat. Sci. Rev. 152, 104–117. https://doi.org/10.1016/j.quascirev.2016.09.019.
Garelick, S., Russell, J.M., Dee, S., Verschuren, D., Olago, D.O., 2021. Atmospheric controls on precipitation isotopes and hydroclimate in high-elevation regions in Eastern Africa since the Last Glacial Maximum. Earth Planet Sci. Lett. 567, 116984. https://doi.org/10.1016/j.epsl.2021.116984.
Gasse, F., Van Campo, E., 1998. A 40,000-yr pollen and diatom record from Lake Tritrivakely, Madagascar, in the southern tropics. Quat. Res. 49, 299–311. https://doi.org/10.1006/qres.1998.1967.
Gasse, F., van Campo, E., 2001. Late Quaternary environmental changes from a pollen and diatom record in the southern tropics (Lake Tritrivakely, Madagascar). Palaeogeogr. Palaeoclimatol. Palaeoecol. 167, 287–308. https://doi.org/10.1016/S0031-0182(00)00242-X.
Gasse, F., Cortijo, E., Disnar, J.-R., Ferry, L., Gilbert, E., Kissel, C., Laggoun-Défarge, F., Lallier-Vergès, E., Miskovsky, J.-C., Ratsimbazafy, B., Ranaivo, F., Robinson, L., Tucholka, P., Saos, J.-L., Sifeddine, A., Taieb, M., Van Campo, E., Williamson, D., 1994. A 36 ka environmental record in the southern tropics : Lake Tritrivakely (Madgascar) (Un enregistrement de l'environnement depuis 36 ka en zone tropicale sud : le lac Tritrivakely (Madagascar)). Comptes Rendus Académie Sci. - Ser. IIA - Earth Planet. Sci. 318, 1513–1519.
Goodman, S.M., Raherilalao, M.J., Wohlhauser, S., 2018. Site 97. Tsimanampesotse. In: The Terrestrial Protected Areas of Madagascar: Their History, Description and Biota. Association Vahatra, Antananarivo, pp. 1650–1666.
Grise, K.M., Davis, S.M., Simpson, I.R., Waugh, D.W., Fu, Q., Allen, R.J., Rosenlof, K.H., Ummenhofer, C.C., Karnauskas, K.B., Maycock, A.C., Quan, X.-W., Birner, T., Staten, P.W., 2019. Recent tropical expansion: natural variability or forced response? J. Clim. 32, 1551–1571. https://doi.org/10.1175/JCLI-D-18-0444.1.
Hersbach, H., Bell, B., Berrisford, P., Hirahara, S., Horányi, A., Muñoz-Sabater, J., Nicolas, J., Peubey, C., Radu, R., Schepers, D., Simmons, A., Soci, C., Abdalla, S., Abellan, X., Balsamo, G., Bechtold, P., Biavati, G., Bidlot, J., Bonavita, M., Chiara, G.D., Dahlgren, P., Dee, D., Diamantakis, M., Dragani, R., Flemming, J., Forbes, R., Fuentes, M., Geer, A., Haimberger, L., Healy, S., Hogan, R.J., Hólm, E., Janisková, M., Keeley, S., Laloyaux, P., Lopez, P., Lupu, C., Radnoti, G., Rosnay, P. de, Rozum, I., Vamborg, F., Villaume, S., Thépaut, J.-N., 2020a. The ERA5 global reanalysis. Q. J. R. Meteorol. Soc. 146, 1999–2049. https://doi.org/10.1002/qj.3803.
Hersbach, H., Bell, B., Berrisford, P., Hirahara, S., Horányi, A., Muñoz-Sabater, J., Nicolas, J., Peubey, C., Radu, R., Schepers, D., Simmons, A., Soci, C., Abdalla, S., Abellan, X., Balsamo, G., Bechtold, P., Biavati, G., Bidlot, J., Bonavita, M., De Chiara, G., Dahlgren, P., Dee, D., Diamantakis, M., Dragani, R., Flemming, J., Forbes, R., Fuentes, M., Geer, A., Haimberger, L., Healy, S., Hogan, R.J., Hólm, E., Janisková, M., Keeley, S., Laloyaux, P., Lopez, P., Lupu, C., Radnoti, G., de Rosnay, P., Rozum, I., Vamborg, F., Villaume, S., Thépaut, J.-N., 2020b. The ERA5 global reanalysis. Q. J. R. Meteorol. Soc. 146, 1999–2049. https://doi.org/10.1002/qj.3803.
IPCC, 2013. In: Stocker, T.F., Qin, D., Plattner, G.-K., Tignor, M., Allen, S.K., Boschung, J., Nauels, A., Xia, Y., Bex, V., Midgley, P.M. (Eds.), Climate Change 2013: the Physical Science Basis. Contribution of Working Group I to the Fifth Assessment Report of the Intergovernmental Panel on Climate Change. Cambridge University Press, Cambridge, United Kingdom and New York, NY, USA, p. 1535. https://doi.org/10.1017/CBO9781107415324. https://www.ipcc.ch/report/ar5/syr/, 10.16.20.
Jaffey, A.H., Flynn, K.F., Glendenin, L.E., Bentley, W.C., Essling, A.M., 1971. Precision measurement of half-lives and specific activities of 235U and 238U. Phys. Rev. C 4, 1889–1906. https://doi.org/10.1103/PhysRevC.4.1889.
Johnson, T.C., Scholz, C.A., Talbot, M.R., Kelts, K., al, et al., 1996. Late Pleistocene desiccation of Lake Victoria and rapid evolution of cichlid fishes. Science 273, 1091.
Jury, M.R., 2003. The climate of Madagascar. In: Goodman, S.M., Benstead, J.P. (Eds.), The Natural History of Madagascar. University of Chicago Press, Chicago, pp. 75–87.
Jury, M.R., 2015. Summer climate of Madagascar and monsoon pulsing of its vortex. Meteorol. Atmos. Phys. 128, 117–129. https://doi.org/10.1007/s00703-015-0401-5.
Jury, M.R., Parker, B.A., Raholijao, N., Nassor, A., 1995. Variability of summer rainfall over Madagascar: climatic determinants at interannual scales. Int. J. Climatol. 15, 1323–1332. https://doi.org/10.1002/joc.3370151203.
Kanner, L.C., Burns, S.J., Cheng, H., Edwards, R.L., 2012. High-latitude forcing of the south American summer monsoon during the last glacial. Science 335, 570–573. https://doi.org/10.1126/science.1213397.
Kiefer, T., McCave, I.N., Elderfield, H., 2006. Antarctic control on tropical Indian Ocean sea surface temperature and hydrography. Geophys. Res. Lett. 33, L24612. https://doi.org/10.1029/2006GL027097.
Koseki, S., Bhatt, B.C., 2018. Unique relationship between tropical rainfall and SST to the north of the Mozambique Channel in boreal winter. Int. J. Climatol. 38, e378–e387. https://doi.org/10.1002/joc.5378.
Lachniet, M.S., 2009. Climatic and environmental controls on speleothem oxygen-isotope values. Quat. Sci. Rev. 28, 412–432. https://doi.org/10.1016/j.quascirev.2008.10.021.
Lau, W.K.M., Kim, K.-M., 2015. Robust Hadley Circulation changes and increasing global dryness due to CO_2 warming from CMIP5 model projections. Proc. Natl. Acad. Sci. 112, 3630. https://doi.org/10.1073/pnas.1418682112.
Ma, Y., Weldeab, S., Schneider, R.R., Andersen, N., Garbe-Schönberg, D., Friedrich, T., 2021. Strong southern African monsoon and weak Mozambique channel throughflow during Heinrich events: implication for Agulhas leakage. Earth Planet Sci. Lett. 574, 117148. https://doi.org/10.1016/j.epsl.2021.117148.
Matsumoto, J., Burney, D.A., 1994. Late Holocene environments at Lake Mitsinjo, northwestern Madagascar. Holocene 4, 16–24. https://doi.org/10.1177/095968369400400103.
Otto-Bliesner, B.L., Russell, J.M., Clark, P.U., Liu, Z., Overpeck, J.T., Konecky, B., deMenocal, P., Nicholson, S.E., He, F., Lu, Z., 2014. Coherent changes of southeastern equatorial and northern African rainfall during the last deglaciation. Science 346, 1223–1227. https://doi.org/10.1126/science.1259531.
Parrenin, F., Masson-Delmotte, V., Köhler, P., Raynaud, D., Paillard, D., Schwander, J., Barbante, C., Landais, A., Wegner, A., Jouzel, J., 2013. Antarctic temperature stack (ATS) from five different ice cores (EDC, Vostok, Dome Fuji, TALDICE, and EDML). Suppl. Parrenin F Al 2013 synchronous change atmospheric CO2 Antarct. Temp. Last Deglacial Warm. Sci. 3396123 1060-1063 Httpsdoiorg101126science1226368. https://doi.org/10.1594/PANGAEA.810188.
Pascale, S., Carvalho, L.M.V., Adams, D.K., Castro, C.L., Cavalcanti, I.F.A., 2019. Current and future variations of the monsoons of the Americas in a warming climate. Curr. Clim. Change Rep. 5, 125–144. https://doi.org/10.1007/s40641-019-00135-w.
Prell, W.L., Kutzbach, J.E., 1987. Monsoon variability over the past 150,000 years. J. Geophys. Res. Atmospheres 92, 8411–8425. https://doi.org/10.1029/

JD092iD07p08411.
Rohling, E.J., Liu, Q.S., Roberts, A.P., Stanford, J.D., Rasmussen, S.O., Langen, P.L., Siddall, M., 2009. Controls on the East Asian monsoon during the last glacial cycle, based on comparison between Hulu Cave and polar ice-core records. Quat. Sci. Rev. 28, 3291–3302. https://doi.org/10.1016/j.quascirev.2009.09.007.
Schefuß, E., Kuhlmann, H., Mollenhauer, G., Prange, M., Pätzold, J., 2011. Forcing of wet phases in southeast Africa over the past 17,000 years. Nature 480, 509–512. https://doi.org/10.1038/nature10685.
Schneider, T., Bischoff, T., Haug, G.H., 2014. Migrations and dynamics of the intertropical convergence zone. Nature 513, 45–53. https://doi.org/10.1038/nature13636.
Scroxton, N., Gagan, M.K., Dunbar, G.B., Ayliffe, L.K., Hantoro, W.S., Shen, C.-C., Hellstrom, J.C., Zhao, J., Cheng, H., Edwards, R.L., Sun, H., Rifai, H., 2016. Natural attrition and growth frequency variations of stalagmites in southwest Sulawesi over the past 530,000years. Palaeogeogr. Palaeoclimatol. Palaeoecol. 441, 823–833. https://doi.org/10.1016/j.palaeo.2015.10.030.
Scroxton, N., Burns, S.J., McGee, D., Hardt, B., Godfrey, L.R., Ranivoharimanana, L., Faina, P., 2017. Hemispherically in-phase precipitation variability over the last 1700 years in a Madagascar speleothem record. Quat. Sci. Rev. 164, 25–36. https://doi.org/10.1016/j.quascirev.2017.03.017.
Scroxton, N., Burns, S.J., McGee, D., Hardt, B., Godfrey, L.R., Ranivoharimanana, L., Faina, P., 2019. Competing temperature and atmospheric circulation effects on southwest Madagascan rainfall during the last deglaciation. Paleoceanogr. Paleoclimatol. 34, 275–286. https://doi.org/10.1029/2018PA003466.
Sharman, G.R., Sharman, J.P., Sylvester, Z., 2018. detritalPy: a Python-based toolset for visualizing and analysing detrital geo-thermochronologic data. Deposit. Rec. 4, 202–215. https://doi.org/10.1002/dep2.45.
Singarayer, J.S., Valdes, P.J., Roberts, W.H.G., 2017. Ocean dominated expansion and contraction of the late Quaternary tropical rainbelt. Sci. Rep. 7. https://doi.org/10.1038/s41598-017-09816-8.
Stager, J.C., Ryves, D.B., Chase, B.M., Pausata, F.S.R., 2011. Catastrophic drought in the afro-Asian monsoon region during Heinrich event 1. Science 331, 1299–1302. https://doi.org/10.1126/science.1198322.
Stríkis, N.M., Cruz, F.W., Barreto, E.A.S., Naughton, F., Vuille, M., Cheng, H., Voelker, A.H.L., Zhang, H., Karmann, I., Edwards, R.L., Auler, A.S., Santos, R.V., Sales, H.R., 2018. South American monsoon response to iceberg discharge in the North Atlantic. Proc. Natl. Acad. Sci. 115, 3788–3793. https://doi.org/10.1073/pnas.1717784115.
Tierney, J.E., Russell, J.M., Huang, Y., Damsté, J.S.S., Hopmans, E.C., Cohen, A.S., 2008. Northern hemisphere controls on tropical southeast African climate during the past 60,000 years. Science 322, 252–255. https://doi.org/10.1126/science.1160485.
Tierney, J.E., Lewis, S.C., Cook, B.I., LeGrande, A.N., Schmidt, G.A., 2011. Model, proxy and isotopic perspectives on the east African humid period. Earth Planet Sci. Lett. 307, 103–112. https://doi.org/10.1016/j.epsl.2011.04.038.
Tierney, J.E., Pausata, F.S.R., deMenocal, P., 2016. Deglacial Indian monsoon failure and North Atlantic stadials linked by Indian Ocean surface cooling. Nat. Geosci. 9, 46–50. https://doi.org/10.1038/ngeo2603.
Vaks, A., Bar-Matthews, M., Ayalon, A., Matthews, A., Halicz, L., Frumkin, A., 2007. Desert speleothems reveal climatic window for African exodus of early modern humans. Geology 35, 831–834.
Vallet-Coulomb, C., Gasse, F., Robison, L., Ferry, L., Van Campo, E., Chalié, F., 2006. Hydrological modeling of tropical closed Lake Ihotry (SW Madagascar): sensitivity analysis and implications for paleohydrological reconstructions over the past 4000 years. J. Hydrol., Water Resour. Reg. Dev.: The Okavango River 331, 257–271. https://doi.org/10.1016/j.jhydrol.2006.05.026.
Voarintsoa, Ny Riavo, G., Wang, L., Railsback, L.B., Brook, G.A., Liang, F., Cheng, H., Edwards, R.L., 2017a. Multiple proxy analyses of a U/Th-dated stalagmite to reconstruct paleoenvironmental changes in northwestern Madagascar between 370CE and 1300CE. Palaeogeogr. Palaeoclimatol. Palaeoecol. 469, 138–155. https://doi.org/10.1016/j.palaeo.2017.01.003.
Voarintsoa, N.R.G., Matero, I.S.O., Railsback, L.B., Gregoire, L.J., Tindall, J., Sime, L., Cheng, H., Edwards, R.L., Brook, G.A., Kathayat, G., Li, X., Michel Rakotondrazafy, A.F., Madison Razanatseheno, M.O., 2019. Investigating the 8.2 ka event in northwestern Madagascar: insight from data–model comparisons. Quat. Sci. Rev. 204, 172–186. https://doi.org/10.1016/j.quascirev.2018.11.030.
Voarintsoa, Gilbertinie, Ny Riavo, Railsback, L.B., Brook, G.A., Wang, L., Kathayat, G., Cheng, H., Li, X., Edwards, R.L., Rakotondrazafy, A.F.M., Madison Razanatseheno, M.O., 2017b. Three distinct Holocene intervals of stalagmite deposition and nondeposition revealed in NW Madagascar, and their paleoclimate implications. Clim. Past 13, 1771–1790. https://doi.org/10.5194/cp-13-1771-2017.
WAIS Divide Project Members, 2015. Precise interpolar phasing of abrupt climate change during the last ice age. Nature 520, 661–665. https://doi.org/10.1038/nature14401.
Wang, Y.J., Cheng, H., Edwards, R.L., An, Z.S., Wu, J.Y., Shen, C.C., Dorale, J.A., 2001. A high-resolution absolute-dated late Pleistocene monsoon record from Hulu Cave, China. Science 294, 2345–2348.
Wang, X., Auler, A.S., Edwards, R.L., Cheng, H., Cristalli, P.S., Smart, P.L., Richards, D.A., Shen, C.C., 2004. Wet periods in northeastern Brazil over the past 210 kyr linked to distant climate anomalies. Nature 432, 740–743.
Wang, P.X., Wang, B., Cheng, H., Fasullo, J., Guo, Z.T., Kiefer, T., Liu, Z.Y., 2014. The global monsoon across timescales: coherent variability of regional monsoons. Clim. Past 10. https://doi.org/10.5194/cp-10-2007-2014, 2007–2052.
Wang, L., Brook, G.A., Burney, D.A., Voarintsoa, N.R.G., Liang, F., Cheng, H., Edwards, R.L., 2019. The African Humid Period, rapid climate change events, the timing of human colonization, and megafaunal extinctions in Madagascar during the Holocene: evidence from a 2m Anjohibe Cave stalagmite. Quat. Sci. Rev. 210, 136–153. https://doi.org/10.1016/j.quascirev.2019.02.004.
Weij, R., Woodhead, J., Hellstrom, J., Sniderman, K., 2020. An exploration of the utility of speleothem age distributions for palaeoclimate assessment. Quat. Geochronol. 60, 101112. https://doi.org/10.1016/j.quageo.2020.101112.
Weldeab, S., Lea, D.W., Oberhänsli, H., Schneider, R.R., 2014. Links between southwestern tropical Indian Ocean SST and precipitation over southeastern Africa over the last 17 kyr. Palaeogeogr. Palaeoclimatol. Palaeoecol. 410, 200–212. https://doi.org/10.1016/j.palaeo.2014.06.001.
Yang, H., Lohmann, G., Lu, J., Gowan, E.J., Shi, X., Liu, J., Wang, Q., 2020. Tropical expansion driven by poleward advancing midlatitude meridional temperature gradients. J. Geophys. Res. Atmospheres 125, e2020JD033158. https://doi.org/10.1029/2020JD033158.